Observation of regional air pollutant transport between the megacity Beijing and the North China Plain

Yingruo Li[1], Chunxiang Ye[1,2], Jun Liu[1], Yi Zhu[1], Junxia Wang[1], Ziqiang Tan[1], Weili Lin[3], Limin Zeng[1], Tong Zhu[1*]

[1]SKL-ESPC and BIC-ESAT, College of Environmental Sciences and Engineering, Peking University, Beijing, 100871, China

[2]Now at School of Chemistry, University of Leeds, Leeds LS2 9JT, UK

[3]Meteorological Observation Center, China Meteorological Administration, Beijing, 100081, China

*Corresponding Author: tzhu@pku.edu.cn

Abstract. Megacities have strong interactions with the surrounding regions through transport of air pollutants. It has been frequently addressed that the air quality of Beijing is influenced by the influx of air pollutants from the North China Plain (NCP). Estimations of air pollutant cross-boundary transport between Beijing and the NCP are important for air quality management. However, evaluation of cross-boundary transport using long-term observations is very limited. Using the observational results of the gaseous pollutants SO_2, NO, NO_2, O_3, and CO from August 2006 to October 2008 at the Yufa site, a cross-boundary site between the megacity Beijing and the NCP, together with meteorological parameters, we explored a method for evaluating the transport flux intensities at Yufa, as part of the "Campaign of Air Quality Research in Beijing and Surrounding Region 2006–2008" (CAREBeijing 2006–2008). The hourly mean ± SD (median) concentration of SO_2, NO, NO_2, NO_x, O_3, O_x, and CO was 15 ± 16 (9) ppb, 12 ± 25 (3) ppb, 24 ± 19 (20) ppb, 36 ± 39 (23) ppb, 28 ± 27 (21) ppb, 52 ± 24 (45) ppb, and 1.6 ± 1.4 (1.2) ppm during the observation period, respectively. The bivariate polar plots showed the dependence of pollutant concentrations on both wind speed and wind direction, and thus inferred their dominant transport directions. Surface flux intensity calculations further demonstrated the regional transport influence of Beijing and the NCP on Yufa. The net surface transport flux intensity (mean ± SD) of SO_2, NO, NO_2, NO_x, O_3, O_x, and CO was 6.2 ± 89.5, -4.3 ± 29.5, -0.6 ± 72.3, -4.9 ± 93.0, 14.7 ± 187.8, 14.8 ± 234.9, and 70 ± 2830 μg s^{-1} m^{-2} during the observation period, respectively. For SO_2, CO, O_3, and O_x the surface flux intensities from the NCP to Yufa surpassed those from Beijing to Yufa in all seasons except winter, with the strongest net fluxes largely in summer, which

was about 4–8 times of other seasons. The surface transport flux intensity of NO_x from Beijing to Yufa was stronger than that from the NCP to Yufa except in summer, with the strongest net flux in winter, which was about 1.3–8 times of other seasons. The flux intensities were then assigned to the corresponding trajectories in the potential source contribution function analysis (PSCF), which confirmed the results of flux intensity calculations. Our study also suggested that various factors, such as the wind field, emission inventory, and photochemical reactions, could influence transport of air pollutants. The decrease of surface flux intensity during the Olympic Games period implied the role of both local emission reduction and regional cooperation in successful air quality management. Three dimensional observations are needed for further comprehensive discussion of the regional transport between Beijing and the NCP.

Keywords: Megacity Beijing, North China Plain, Yufa site, Regional transport, Long-term and multiple-species observation

1. Introduction

Megacities are large sources of air pollutants and greatly influence the surrounding areas (Parrish and Zhu, 2009). With a population over 20 million, the city of Beijing is an example of such a megacity. Beijing has faced severe air pollution problems over the past two decades and has intensive interactions with other emission hot spots within the North China Plain (NCP) (Chen et al., 2015; Shao et al., 2006; Zhang et al., 2012). Beijing and the NCP are surrounded by the Yanshan Mountains to the north and the Taihang Mountains to the west. The semi-basin geographical features

63 together with the continental monsoon climate make regional transport of air
64 pollutants between the megacity Beijing and the NCP an important factor affecting
65 air quality in Beijing and the NCP (An et al., 2007; Guo et al., 2010; Lin et al., 2008,
66 2009; Streets et al., 2007; Wang et al., 2006; Wang et al., 2011; Wang et al. 2015; Wu
67 et al., 2011; Xu et al., 2005; Xu et al., 2011). An improved understanding of the
68 regional transport of air pollutants between Beijing and the NCP is therefore
69 essential for air quality management of the megacity Beijing and establishment of
70 regional-scale emissions control measures.

71 Previous studies have shed light on the regional transport sources of the
72 megacity Beijing, and various techniques have been employed, including rural/urban
73 station observations (Guo et al., 2010; Lin et al., 2008, 2009; Wang et al., 2006; Xu et
74 al., 2011), mobile laboratory measurements (Wang et al., 2009, 2011; Zhu et al.,
75 2016), and modelling studies (An et al., 2007; Matsui et al., 2009; Wu et al., 2011). A
76 ground-based observation study from July 2006 to September 2007 at the Gucheng
77 site (Lin et al., 2009), a rural site south-west of Beijing, found that high
78 concentrations of gaseous pollutants, including nitric oxide (NO), nitrogen dioxide
79 (NO_2), nitrogen oxides (NO_x=NO+NO_2), sulphur dioxide (SO_2), carbon monoxide (CO),
80 ozone (O_3), and oxidant (O_x=NO_2+O_3), were accompanied by air masses moving
81 northward from Gucheng to Beijing, according to back-trajectory analysis. Similar to
82 Lin et al. (2009), regional transport of air pollutants between Beijing and the NCP was
83 observed consistently in these previous studies (Lin et al., 2008; Yuan et al., 2009;
84 Zhu et al., 2011), even though they were merely short-term observations.

Many studies have also attempted to quantify transport fluxes of the main gaseous pollutants. A mobile laboratory study in Beijing city demonstrated regional transport of SO_2 from the NCP in both emission-control and non-control scenarios during the Beijing 2008 Olympics (Wang et al., 2011). Extrapolated from five 1-day case studies, the annual transport fluxes of SO_2 through the south-east part of the 6th Ring Road into Beijing were estimated at 49.2 Gg yr^{-1} and 146.3 Gg yr^{-1}, accounting for 70 % and 73 % of the annual SO_2 emissions in Beijing under emission-control and non-control scenarios, respectively. The Community Multi-scale Air Quality (CMAQ) model simulation by An et al. (2007) found that the regional transport from the surrounding areas of Beijing contributed 39 % of $PM_{2.5}$, 30 % of PM_{10}, and 18 % of SO_2 to the city on average in a heavy pollution episode in the spring of 2005. Similarly, the CMAQ model simulation over the Beijing region for July 2001, reported by Streets et al. (2007), illustrated the regional transport of $PM_{2.5}$ and O_3 between Beijing and the NCP. The study suggested that the average contributions of regional transport to $PM_{2.5}$ concentrations in the megacity Beijing from Hebei Province, Shandong Province, and Shanxi Province were about 32 %, 11 %, and 3.5 %, with maximum contributions of 70 %, 63 %, and 21 %, respectively. The regional transport contributions to the concentrations of O_3 in Beijing were less significant, with maximum contributions of 28 % from Hebei Province, 24 % from Shandong Province, and 10 % from Shanxi Province, respectively.

In summary, long-term observation of transport flux is necessary to constrain regional models and to directly evaluate the influence of regional transport on air quality. Estimations of air pollutant cross-boundary transport between Beijing and

the NCP are important for air quality management. However, evaluation of cross-boundary transport using long-term observations is very limited. In this study, we developed a method of calculating the surface transport flux intensity across a cross-boundary site based on long-term ground-based measurement and evaluated the regional transport influence of Beijing and the NCP on the cross-boundary site. The results showed different transport directions and seasonal variations in the surface transport flux intensities of the main pollutants, including SO_2, NO, NO_2, NO_x, O_3, and CO at the Yufa site. The key factors controlling regional transport are also discussed, which is important for the establishment of air quality control policy in future.

2. Measurements and Methods

2.1. Measurements

The Yufa site is located at the cross-boundary area between Beijing and the NCP and could be influenced by emissions from the megacity Beijing and long-range transport from the NCP. The measurements at the Yufa site (39°30'49"N, 116°18'15"E) were conducted on the top of a building (about 20 m above ground level) in the campus of Huangpu College. There is no tall building around the Yufa site which affects the wind and gaseous pollutant measurements. This is a rural site about 50 km south of the center of Beijing and near the border of Beijing Municipality and Hebei Province. As shown in Fig. 1, the Yufa site locates in the temperate monsoon climate zone and the topography of its surrounding area is flat. The prevailing wind of the Yufa site is the same as the surrounding region (Lin et al., 2009), thus the wind field of the Yufa site is representative of the researched area in this study. The northern and western sides

130 of the site are mountain areas where dry and clean air masses come from, whereas
131 the southern and south-eastern sides are surrounded by heavily industrialised and
132 urbanised areas, such as Hebei Province and Tianjin City (Fig.1).

133 Figure 1. here

134 The gaseous pollutant species measured included SO_2, NO, NO_2, NO_x, O_3, and CO.
135 SO_2 was measured using a sulphur dioxide analyser (9850B; Ecotech, Knoxfield,
136 Australia) which combines microprocessor control with pulsed UV fluorescence
137 detection with the precision of 0.5 ppb and uncertainty within 10 %. The detection
138 limit for the analyser is 0.5 ppb and the time resolution is 1 min. Reactive nitrogen
139 species (NO, NO_2, and NO_x) were measured using nitrogen analyser (9841B; Ecotech)
140 which utilises microprocessor control and chemiluminescence detection with the
141 precision of 0.5 ppb and uncertainty within 10 %. The detection limit for the
142 instrument is 0.5 ppb and the time resolution is 1 min. CO was measured using a CO
143 analyser (9830A; Ecotech) which utilises NDIR Gas Filter Correlation photometry and
144 microprocessor control with the precision of 0.1 ppm and uncertainty within 1 %.
145 The detection limit for the instrument is 50 ppb and the time resolution is 1 min. O_3
146 was measured using an ozone analyser (9810B; Ecotech) which combines
147 microprocessor control with UV photometry with the precision of 1 ppb and
148 uncertainty within 5 %. The detection limit for the instrument is 0.4 ppb and the time
149 resolution is 1 min. Measurements of meteorological parameters, including wind
150 direction (WD), wind speed (WS), temperature (T), barometric pressure (BP), and
151 relative humidity (RH), were conducted with a LASTEM auto meteorology station
152 (LASTEM, Milan, Italy). All trace gas instruments were maintained and calibrated

routinely following the manufacturer's protocols. The main reasons for missing data were power and instrument failure. The detail information of the instruments was listed in Table 1.

Table 1. here

2.2. Methods

2.2.1. Transport direction analysis

The transport of gaseous pollutants is markedly influenced by meteorological parameters, especially wind speed and wind direction. For local emission sources, wind can facilitate the dilution and diffusion of air pollutants. Strong wind usually has marked diffusion capability, whereas weak wind usually leads to accumulation of air pollutants. For regional sources, strong wind can transport pollutants over long distances and may result in high concentrations of pollutants in downwind areas. Therefore, the relationship between pollutant concentration and wind field is an indicator of regional transport.

The bivariate polar plot graphical technique was used to investigate the relationships between the concentrations of gaseous pollutants and wind field, and to identify potential emissions sources and transport directions of air pollutants according to the technique developed by Carslaw et al. (2006) and Westmoreland et al. (2007). The variables (such as pollutant concentrations, wind speed, and wind direction) were plotted in polar coordinates. The procedure was as follows. First, the concentration data were partitioned into wind speed-wind direction bins, and the

mean concentrations were calculated within each bin. Then, the wind components *u* and *v* were calculated using Eq. (1):

$$u = \mathrm{WS} \cdot \sin(\pi\theta/180), v = \mathrm{WS} \cdot \cos(\pi\theta/180) \quad (1),$$

where *WS* is the hourly mean wind speed, and ϑ is the wind direction in degrees, with 90° being from the east. Then, a generalised additive model (GAM; Jayamurugan et al., 2013) was used for surface fitting to describe the concentration as a function of the wind components *u* and *v*. The concentrations calculated by the GAM can be expressed with Eq. (2):

$$\sqrt{C_i} = \beta_0 + s(u, v) + e_i \ (2),$$

where C_i is the calculated pollutant concentration, β_0 is the overall mean of the response, $s(u,v)$ is the smooth function, and e_i is the residual.

Compared to the nonparametric regression used by Henry et al. (2002), the bivariate polar plot involves the dependence of pollutant concentration on both wind speed and wind direction. The non-linear relationships among the variables (such as concentrations of gaseous pollutants, wind speed, and wind direction) as well as the interactions among these variables can be considered using the GAM method for data smoothing. In addition, the use of polar coordinates makes the graphics more intuitive.

2.2.2. Transport flux assessment

The surface transport fluxes at the Yufa site were calculated with the following formula (White et al., 1976; Wang et al., 2011):

$$f = -\frac{1}{n}\sum_{j=1}^{n} C_j \times WS_j \times cos\theta_j \quad (3),$$

196 $$\sigma = H_0 \times L_0 \quad (4),$$

197 $$FLUX = f \times \sigma \quad (5),$$

198 where f is surface flux intensity of the pollutants, i.e. the per unit area flux (μg s^{-1}
199 m^{-2}); C_j is the mean concentration of the pollutants (μg m^{-3}) during the jth
200 observation hour; ϑ_j is the angle between wind direction and the north-south
201 direction during the jth observation hour; and WS_j is wind speed (m s^{-1}) during the
202 jth observation hour; n is the total number of observation hour; σ is the surface
203 cross-sectional area (m^2) with the width of L_0 (m) and height of H_0 (m); the average
204 surface flux of the pollutants (i.e. *FLUX*, μg s^{-1}) can be obtained by multiplying flux
205 intensity f and the cross-section area σ.

206 Figure S1 shows a schematic diagram of the surface flux calculation. The flux
207 intensity here is the product of wind vector and air pollutant concentration
208 measured at the same location. Ideally, we need to use the wind speed and air
209 pollutant concentration with infinite small time resolution to conduct the surface flux
210 calculations. In this study, the hourly data of the pollutants and wind were used,
211 mainly because the pollutants concentration data was converted from the minutes'
212 data to hourly mean to remove the accidental fluctuation and reduce the noise.
213 Therefore, we assumed the wind speed and wind direction were constant within one
214 hour, and hourly wind data was used to match with the hourly air pollutant
215 concentration data to calculate the flux intensity.

216 It also need to make it clear that the surface flux intensity calculated in this study
217 is the per unit area flux across the Yufa site, which is different from the flux across a
218 large area reported in other studies (e.g. Wang et al. 2011). Our results could only be

extrapolated if the concentrations of all the pollutants, wind speed and direction were homogenously distributed, vertically and horizontally. Otherwise, vertical profiles of air pollutants concentration and wind are needed to calculate the cross-section transport flux of two adjacent regions for the whole boundary layer with the integrating formula below:

$$FLUX = \iint C_{(x,z)} WS_{(x,z)} sin\theta_{(x,z)} dxdz = \iint f_{(x,z)} dxdz \quad (6),$$

where x is horizontal distance to the observed point, z is the vertical distance from ground to the observed point. In this study, we focus on the method developing of the surface flux intensity calculation and evaluation of the regional transport influence of Beijing and the NCP on the cross-boundary site based on the ground-based observation data.

2.2.3 The backward trajectory model and PSCF analysis

The 12 h air mass back trajectories arriving at the Yufa site at 500 m above the ground level were calculated using the National Oceanic and Atmospheric Administration (NOAA) Hybrid Single-Particle Lagrangian Integrated Trajectory Version 4 model (HYSPLIT-4 model) (http://ready.arl.noaa.gov/HYSPLIT.php) during the study period (from 15 August 2006 to 31 October 2008) with a 1 ˚ × 1 ˚ latitude-longitude horizontal resolution and the final meteorological database. The final archived meteorological data was obtained from the National Center for Environmental Prediction's (NCEP's) Global Data Assimilation System (GDAS) (ftp://arlftp.arlhq.noaa.gov/pub/archives/gdas1). The back trajectories were

generated with 6-h time resolution (four times per day) at starting times of 0:00, 6:00, 12:00 and 18:00 UTC (8:00, 14:00, 20:00, 4:00 LT-local time, respectively).

The potential source contribution function (PSCF) analysis was performed with the Gis-based software TrajStat (http://www.meteothinker.com/products/trajstat.html) (Wang and Zhang et al., 2009). The PSCF analysis has been widely used for identifying the possible source areas of the observed high concentrations of pollutants at the receptor site (Ashbaugh et al., 1985; Zhang et al., 2013). In this study the long-term calculated surface flux intensity data was assigned to the backward trajectories in the PSCF analysis to confirm the bi-directional transport of pollutants between Beijing and the NCP. The PSCF analysis was conducted as follows.

The study domain was divided into i × j equal size grid cells and the PSCF value for *ij*th cell is defined as:

$$\mathrm{PSCF}_{ij} = m_{ij} / n_{ij} \quad (7),$$

where n_{ij} denoted the number of endpoints that fall in the *ij*th cell, and m_{ij} represented the number of endpoints for the same cell having arrival times at the observed site corresponding to measured data higher than an arbitrarily set criterion.

To reduce the effect of small values of n_{ij}, the PSCF values were multiplied by an arbitrary weigh function W_{ij}. In this study, W_{ij} is defined as below.

$$W_{ij} = \begin{cases} 1.00, & 80 < n_{ij} \\ 0.70, & 20 < n_{ij} \leq 80 \\ 0.42, & 10 < n_{ij} \leq 20 \\ 0.05, & n_{ij} \leq 10 \end{cases} \quad (8),$$

In this study, the study domain was 30–50 ˚ N, 100–125 ˚ E and the horizontal resolution was 0.25 ˚ × 0.25 ˚.

3. Results and discussion

3.1. Observations

Figure 2. here

The time series of hourly average and 24-hour smoothing concentrations of SO_2, NO, NO_2, NO_x, O_3, O_x, and CO observed at the Yufa site from 15 August 2006 to 31 October 2008 are shown in Fig. 2. The hourly mean ± SD (median) concentration value of SO_2, NO, NO_2, NO_x, O_3, O_x, and CO was 15 ± 16 (9) ppb, 12 ± 25 (3) ppb, 24 ± 19 (20) ppb, 36 ± 39 (23) ppb, 28 ± 27 (21) ppb, 52 ± 24 (45) ppb, and 1.6 ± 1.4 (1.2) ppm during the observation period from 01 September 2006 to 31 August 2008, respectively, with hourly mean values -3, 1, 6, 7, -1, 5 and 0 ppb higher for SO_2, NO, NO_2, NO_x, O_3, O_x, and CO than the Gucheng site, a polluted rural site to the south-west of Beijing, from July 2006 to September 2007 (Lin et al., 2009). The hourly mean values were 12, 11, 17, 28, -5, 22 and 972 ppb higher than those observed at the clean background at the Shangdianzi site, which is one of the regional Global Atmosphere Watch (GAW) stations in China over the period 2004–2006 (Lin et al., 2008). The compared results indicated that the Yufa site has become a relatively polluted rural site. Typical seasonal variations were observed for all gaseous pollutants. Concentrations of primary pollutants, including SO_2, NO, NO_2, NO_x, and CO, were high in winter and low in summer. In contrast, the concentration of O_3, which is a secondary pollutant, was high in summer and low in winter.

Figure 3. here

282 Meteorological parameters such as WS, WD, RH, T, and BP were also measured
283 at the Yufa site; the monthly statistics are shown in Fig. 3. North (usually in winter) or
284 south wind (usually in summer) prevailed at the Yufa site, with monthly average wind
285 speed mostly below 2 m s^{-1}. Exceptional conditions occurred occasionally in spring
286 and winter for the north wind, with monthly average wind speeds around 2–3 m s^{-1}.
287 In addition, for the north wind, the mean speed was higher than the median speed,
288 suggesting the prevalence of high wind speeds in both spring and winter. Prevailing
289 north wind with high wind speed during winter and spring has been reported
290 consistently in the Beijing area (Lin et al., 2008; Wehner et al., 2008). Another
291 exceptional condition occurred in spring for the south wind, with a monthly average
292 wind speed around 2 m s^{-1}. Figure 4 summarises the prevalence of wind direction in
293 the four seasons. Generally, the prevailing surface wind directions were north-
294 northeast and south-southwest in all seasons. In winter and spring, winds from the
295 north-northeast sector made a contribution of about 40–50 % to wind frequency.
296 Whereas under the influence of summer monsoon, winds from south increased
297 significantly in summer, with the contribution to wind frequency above 40 %. RH was
298 higher in summer and lower in spring and winter with the driest month in April of
299 2007 and February of 2008. The seasonal variation of RH may partially be related to
300 the variations of WS (Lin et al., 2011). T was higher in summer and lower in winter.
301 Surface pressure measurements showed high values in winter and low values in
302 summer due to surface heating and lifting air masses in summer, which partly
303 accounted for the wind field in the NCP (Takegawa et al., 2009).

304 Figure 4. here

305 The seasonal variations in gaseous pollutants and meteorological parameters
306 could be linked in certain ways. For example, the high temperature and low pressure
307 in summer suggested a high boundary layer and diluted gaseous pollutants to some
308 extent. The high temperature, light intensity, and relative humidity also favoured the
309 chemical transformation of these primary pollutants and the formation of secondary
310 pollutants. The high wind speeds in spring and winter also affected regional
311 transport, and therefore the concentrations of gaseous pollutants, as discussed
312 below.

313 **3.2. Transport direction**

314 **3.2.1. The bivariate polar plots for the whole observed period**

315 As shown in Fig. 1, the Yufa site is located at the boundary area of Beijing city and the
316 NCP. Prevalent south/south-west or north/north-east wind would bring in polluted or
317 clean air masses to the site. Air masses from both directions would pass over the
318 Yufa site. Regional transport from the megacity Beijing and the NCP could therefore
319 be observed at the Yufa site. The transport directions for gaseous pollutants,
320 including SO_2, NO, NO_2, NO_x, O_3, O_x, and CO, will be discussed in this section.

321 Figure 5. here

322 Figure 5a-g show the bivariate polar plots for SO_2, NO, NO_2, NO_x, O_3, O_x, and CO
323 at the Yufa site, respectively. In the low wind speed scenario, high or medium
324 concentrations of NO, NO_2, NO_x, SO_2, and CO were generally observed, along with
325 low O_3 and O_x concentrations. In the high wind speed scenario, the dependence of
326 species concentration on wind speed and wind direction was more varied.

Specifically, the bivariate polar plot in Fig. 5b clearly shows dependence of high NO concentration (higher than 30 ppb) on low wind speed, with low NO concentration (lower than 5 ppb) at wind speeds > 3 m s^{-1}. The bivariate polar plot in Fig. 5c shows similar dependence of high NO_2 concentration on low wind speed, but NO_2 concentrations up to 20 ppb were still observed with medium wind speeds of around 5 m s^{-1} from the south, east, and north-east. Accordingly, the dependence pattern of the NO_x concentration (Fig. 5d) on wind speed and wind direction reflected the features of both NO and NO_2. The dependence pattern of high CO concentration on low wind speed in Fig. 5g was similar to that for NO_x, but a considerable CO concentration, substantially higher than background level, was still observed at wind speeds exceeding 5 m s^{-1} from the south and the east. Figure 5a shows similar dependence of medium-high concentration of SO_2 (around 20 ppb) on low wind speed, with one unique feature being that high SO_2 concentration was observed under conditions of high wind speed (> 5 m s^{-1}) in various wind directions (especially the south wind). Finally, the bivariate polar plot in Fig. 5e shows the dependence of O_3 concentration on wind speed and wind direction, which was somewhat opposite to the patterns for other species. The low O_3 concentration (< 20 ppb) was related to low wind speed or calm wind conditions. With the north wind and medium or high wind speed, a typical background O_3 concentration (around 50 ppb) was observed. With south wind and medium or high wind speed, high O_3 concentration was observed. The dependence of the high O_x concentration on high wind speed from the south and south-east was similar to that of O_3, but no low concentration of O_x was

observed under low wind speed conditions (Fig. 5f), probably due to the compensation of high NO_x concentration at low wind speeds (Fig. 5d).

Figure 6. here

The high concentrations of NO, NO_2, NO_x, and CO and the medium-high concentration of SO_2 observed under low wind speed conditions were consistent with their high emission intensities in the Beijing area (Fig. 6). Due to the marked increase in the number of vehicles and heavy energy consumption, Beijing has been a well-known emission hot spot for NO and NO_2 (Tang, 2004). Meanwhile, the extremely high levels of CO emissions in the Beijing area are clearly shown in the emissions map (Fig. 6) and have been reported consistently (Wang et al., 2009) and directly observed, with peak CO concentrations up to 9.3 ppm. Only medium-high SO_2 concentration (~15 ppb) observed even at low wind speed suggested the successful reduction of SO_2 emission, which could be ascribed to the continuous effort of the Chinese government since the 1990s and during the Olympic Games (Qin et al., 2009; Tang, 2004; Wang et al., 2009, 2011). Accordingly, the O_3 concentration under low wind speed conditions was lower than the typical background level, which could be attributed to the rapid titration of O_3 by of accumulation NO.

3.2.2. Seasonal variations of the bivariate polar plots

Figure 7. here

The different patterns of the bivariate polar plots reflected the differences in local emission and regional transport for different species. The emissions, the

meteorological conditions, the chemical reaction rate and the species lifetime, which have essential influence on the regional transport, vary greatly by seasons. Thus the seasonal variations of the bivariate polar plots and the corresponding causes were discussed in this section.

Figure 7b-d show seasonal variations of the bivariate polar plots for NO, NO_2, and NO_x at the Yufa site, respectively. Generally, the mean concentrations of NO_2, NO_x and especially NO in the low wind speed scenario were higher than those in the higher wind speed scenario in all seasons. The mean concentration of NO was less than 10 ppb when the wind speed higher than 5 m s^{-1} in all seasons (Fig. 7b). Figure 7c clearly shows the relatively higher concentration of NO_2 (~20 ppb) with winds at higher wind speed (> 5 m s^{-1}) from the south sector in spring, from the northeast and south sectors in summer and winter, and from the northeast sector in autumn. Figure 7d shows the dependence pattern of NO_x was similar to both NO and NO_2. Although emission hot spots of NO, NO_2, and NO_x are widespread in the NCP, the long-range transport of these species to Yufa is limited by the lifetime of these species. As the average O_3 concentration for spring, summer, autumn and winter was 20, 11, 32, and 42 ppb respectively at Yufa, the typical lifetime of NO was 66, 51, 106, and 181 s in spring, summer, autumn, and winter, respectively, just by assuming that all the NO is removed mainly by chemical reaction with O_3 (Sander et al., 2011). The transport distance of NO was therefore less than 5 km even with a high wind speed of 15 m s^{-1}. Even when considering the the conversion of NO from NO_2 with conversion efficiency ~30 % in summer and autumn (Takegawa et al. 2009), the transport distance of NO is still limited, for the lifetime of NO_2 is also relative short

394 (Beirle et al., 2011; Gu et al., 2013). That is, NO concentration is determined by local
395 emissions rather than regional transport. NO_2 and NO_x have longer lifetimes in the
396 atmosphere than NO has, typically on the order of 4–5 h and with longer
397 photochemical lifetime in cold seasons (Beirle et al., 2011; Gu et al., 2013). Hence,
398 the typical transport distance of these species is around 100 km at the wind speed of
399 5 m s^{-1} (Beirle et al., 2011). Within such transport distance, the Yufa site is
400 surrounded by various NO_x emission hot spots (Fig. 6), such as the megacity Beijing
401 to the north, the Baoding-Cangzhou area to the south, and the Tianjin-Tangshan area
402 to the east. Meanwhile the emission intensity was larger in winter and autumn than
403 that in spring and summer (Fig. 6). It is therefore reasonable to observe the influence
404 of short-range transport, in addition to local emissions, on the local NO_2 and NO_x
405 concentrations, especially in cold seasons (Fig. 7c and 7d). Although our results
406 suggested that short-range transport from these surrounding areas, especially the
407 urban area of Beijing, was a non-negligible factor affecting the NO_x concentration at
408 the Yufa site, the regional transport of NO_x was of less significance compared to SO_2
409 and CO due to its limited transport distance (see below).

410 Figure 7e is the seasonal bivariate polar plots of CO, which clearly shows the
411 relatively higher mean concentration of CO (> 1 ppm) with winds at low wind speed
412 (< 2 m s^{-1}), similar to nitrogen oxide species. The mean concentration of CO was
413 relatively higher with wind at higher wind speed (> 5 m s^{-1}) from south sector in
414 spring and summer, from northeast and south sector in autumn, and from north and
415 south in winter. The oxidation lifetime of CO is typically ~20 days, under the
416 assumption of OH radical concentration of 2×10^6 cm^{-3} (Xu et al., 2011). This is

417 substantially longer than the lifetime of NO_x, making regional transport of CO an
418 important process affecting local air quality in the downwind area. The different
419 lifetimes of CO and NO_x appeared to explain the unique high concentration of CO,
420 but not NO_x, at wind speeds exceeding 5 m s^{-1} from the south and the east. Our
421 results suggest that regional transport from the south and central NCP and the
422 Tianjin area could greatly affect local concentrations of CO at the Yufa site.

423 Figure 7a clearly shows the relatively higher mean concentration of SO_2 (~20 ppb)
424 with winds at higher wind speed (> 5 m s^{-1}) from the south sector in spring and
425 summer. The mean concentration of SO_2 was high (> 30 ppb) with winds at higher
426 wind speed (> 5 m s^{-1}) from the north-east, east, and south sectors in autumn and
427 winter. Similar to CO, SO_2 has a relatively long lifetime in the atmosphere compared
428 to NO_x, i.e. a couple of hours to 1–2 days with longer lifetime in winter and shorter
429 lifetime in summer (Beirle et al., 2014; He et al., 2012; Lee et.al., 2014), and regional
430 transport of SO_2 was expected to occur. Accordingly, regional transport from
431 emission hot spots located south of the Yufa site (Fig. 6), was found to influence the
432 concentrations of SO_2 (Fig. 7a) at Yufa in all seasons. Specifically, the highlighted
433 emission hot spots in the central NCP and the south NCP, which accounted for about
434 70 % of China's coal consumption in 10 % of China's domestic area (China Statistical
435 Yearbook, 2008), is a major source of SO_2 in the Beijing area by regional transport
436 (Liu et al., 2016). Furthermore, regional transport from the north-east sector of the
437 Yufa site, where the center of the megacity Beijing located, also was observed in
438 autumn and winter, which indicated the increased emission of SO_2 in heating
439 seasons.

Finally, the bivariate polar plots in Fig. 7f and 7g show the dependence of O_3 and O_x concentration on wind speed and wind direction by season. The low O_3 concentration (< 20 ppb) was observed at low wind speed (< 2 m s^{-1}). With the north wind at higher wind speed (> 5 m s^{-1}), a typical background O_3 concentration (around 50 ppb) was observed in spring and summer. With south wind at higher wind speed (> 5 m s^{-1}), high O_3 concentration (above 60 ppb) was observed, especially in summer. The main difference of seasonal bivariate polar plots between O_3 and O_x was that no low concentration of O_x was observed under low wind speed conditions in all seasons. The low concentration of O_3 at low wind speed may be due to the titration of O_3 by NO, which was more obvious in autumn and winter. Background O_3 levels in the north-west wind under medium and high wind speed conditions clearly reflect the transport of background air mass to the Yufa site from locations where the emission intensities of pollutants were relatively low (Fig. 6), and this was more obvious in spring when the air masses from the north-west increased (Fig. 4). Whereas O_3 concentrations higher than background level in the south wind under medium and high speed conditions, especially in summer, suggest accumulation of O_3 during its transport from the central NCP area or even the south NCP area to the Yufa site. Emission intensity of O_3 precursors, such as NO_x and VOCs is high in the NCP, and the solar radiation is strong in summer, which facilitate the formation and transport of O_3 from the NCP to Beijing (Zhang et al., 2014).

In conclusion, the emissions in the Beijing area are closely related to the observed concentrations of NO, NO_2, NO_x, and CO at Yufa. Regional transport had a clear influence on the concentrations of all gaseous pollutants examined here, with

463 the exception of NO. The emission hot spots located east, north-east, and especially
464 south of the Yufa site determined the regional transport directions. The influence of
465 regional transport differed among species. Regional transport of SO_2, CO, and O_3
466 from the central and south NCP to the Yufa site was more important, whereas
467 regional transport of NO_x from the NCP was less evident. Factors affecting regional
468 transport included, but were not limited to, the atmospheric lifetime of pollutants,
469 wind field, and local and regional emissions. As the Yufa site is a cross-boundary rural
470 site between the megacity Beijing and the NCP, observation of transport flux there is
471 appropriate in evaluating the regional transport influence by both the megacity
472 Beijing and the NCP on the Yufa site.

473 **3.3. Transport flux**

474 To evaluate the surface transport of the main air pollutants from Beijing and the
475 NCP to the Yufa site, the surface flux intensities were calculated with Eqs. (3) based
476 on observations at the Yufa site. The mean net surface flux intensities in each
477 season were also calculated for the 2-year observation period (Table 2). The overall
478 net surface flux intensities (mean ± SD) of SO_2, NO, NO_2, NO_x, O_3, O_x, and CO were
479 6.2 ± 89.5, -4.3 ± 29.5, -0.6 ± 72.3, -4.9 ± 93.0, 14.7 ± 187.8, 14.8 ± 234.9, and 70 ±
480 2830 μg s^{-1} m^{-2} during the observation period from 01 September 2006 to 31
481 August 2008, respectively. The large standard deviation of the surface flux intensity
482 indicated the large variations of the transport flux intensities. Table 3a shows the
483 mean influx intensities (positive; from the NCP to Yufa) were highest in winter and
484 lowest in summer, with the flux intensity values in winter 2–6 times of those in
485 summer. The outflux intensities (negative; from Beijing to Yufa) show the same

pattern, with the absolute flux intensity values in winter 2–8 times of those in summer (Table 3b). Yet the overall net transport surface flux intensities show quite different seasonal variations (Table 2) comparing to the results in Table 3. For SO_2, CO, O_3, and O_x the surface transport flux intensities from the NCP to Yufa surpassed those from Beijing to Yufa in all seasons except in winter, with the strongest net fluxes largely appeared in summer, which was about 4–8 times of other seasons. The net surface transport flux intensity of NO_x from Beijing to Yufa was stronger than that from the NCP to Yufa except in summer, with the strongest net flux in winter, which was about 1.3–8 times of other seasons.

Table 2. here

Table 3. here

To understand the transport fluxes reported here, it is necessary to discuss the affecting factors. First, the prevalent wind is a dominant factor affecting the surface fluxes. Figure 8 shows the time series of daily average surface flux intensity, i.e. the per unit cell flux (μg s^{-1} m^{-2}) of SO_2, NO, NO_2, NO_x, O_3, O_x, and CO, and corresponding wind vectors (m s^{-1}) during the observation period. In general, the variations in the pollutant flux intensities showed a saw-teethed pattern, with influx (positive; from the NCP to Yufa) and outflux (negative; from Beijing to Yufa) prevailing according to the shift in wind direction. Meanwhile, mainly due to the seasonal variations in wind speed and wind direction (Fig. 3 and 4), the magnitude of surface fluxes showed similar seasonal variation (Table 2). High net positive influx intensities were observed in summer, and high net negative outflux intensities in

508 winter. As the north wind prevailed significantly over the south wind in winter, and
509 the south wind over the north wind in summer (Fig. 4), the values of net surface
510 flux intensities in these two seasons were the highest. During the other two
511 seasons, frequent changes in positive and negative fluxes tended to cancel each
512 other out, making the net transport fluxes less significant. This dominant role of
513 wind field could also be illustrated by conditions during the winter of 2006/07 and
514 2007/08. Exceptionally, the south wind prevailed in the winter of 2006/07 (Fig. 4),
515 leading to the surface flux intensity of pollutants more positive in the winter of
516 2006/07 than 2007/08 (Table 2). For example, the increase of influx intensity for
517 SO_2, NO, NO_2, NO_x and CO between winter of 2006/07 and 2007/08 was on the
518 order of a factor of 1.5 (Table 3a).

519 Figure 8. here

520 Second, the transport flux is determined not only by the wind field but also by
521 the emissions of pollutants in the upwind area. Various pollutants showed different
522 patterns of seasonal variations in flux as a result of relative high emission intensities
523 in the upwind area compared to local emissions. For example, the seasonal surface
524 flux intensities of SO_2 were mainly positive influx, except in winter of 2007/08. The
525 significant regional transport of SO_2 from the NCP to Yufa in all seasons except
526 winter could be partly attributed to the high emission intensity of SO_2 in the NCP
527 (Fig.6) and the reduction of SO_2 emission in Beijing (Qin et al., 2009; Wang et al.,
528 2009, 2011), whereas the SO_2 outflux from Beijing to Yufa was determined by the
529 prevalent north wind, as explained above. In contrast to the net positive influx of
530 SO_2, the net seasonal surface flux intensities of CO were negative in both winter

and autumn. The small outflux of CO in autumn reflected increased CO emission in Beijing, which was sufficiently strong to account for the strong CO emissions in the NCP.

The influence of emissions on transport flux could also be inferred from an emissions-reduction scenario. For example, the 29th Olympic Games was held in Beijing during the period from 8 August 2008 to 20 September 2008. The Beijing government implemented aggressive long- and short-term air quality control measures in Beijing and its surrounding areas before and during the Olympic period to maintain good air quality during the Olympic Games (Wang et al., 2010; Wang et al., 2011). The control measures included moving the heavy polluted factories out the Beijing city, reducing the traffic emission through an odd/even plate number rule, and freezing construction activities (Wang et al., 2009). The concentrations of pollutants and the surface flux intensities during the 2008 Olympic Games were substantially reduced compared to the corresponding period of 2007 (Table 4). Besides the favored meteorological conditions (Fig. S2), the significant emission reduction both in the Beijing area and the NCP during the 2008 Beijing Olympic Games played a key role in the decrease of the transport flux intensities (Zhou et al., 2010).

Table 4. here

Finally, the chemical properties of these species could also affect the flux. Take O_3 for example, although both Beijing and the NCP are regarded as emissions hot spots for O_3 precursors, the short distance between Beijing and the Yufa site may hinder the secondary formation of O_3 to some extent. Thus the surface transport of

554 O_3 from to the NCP to Yufa was stronger than that from Beijing to Yufa, especially in
555 summer time with a net average surface flux intensity value of about 60 μg s^{-1} m^{-2},
556 which is 4–9 times of that in autumn and spring (Table 2). The lifetime of the
557 pollutants also determined the different net transport flux intensities for different
558 species (Table 2 and 3), with the net transport of NO, NO_2 and NO_x from Beijing to
559 Yufa and the net transport of SO_2, CO, O_3 and O_x from the NCP to Yufa. These results
560 are consistent with bivariate polar plots analysis mentioned above (Fig. 5 and 7).

561 Overall, the flux intensities are influenced by at least the wind field, emissions
562 inventory in both the megacity Beijing and the NCP, and the chemical fates of these
563 pollutants in the atmosphere. These observations provide insight for the analysis of
564 projected transport flux under various emissions-reduction scenarios in the future.
565 On the other hand, the dependence of the fluxes on these factors, which can vary,
566 suggests that the fluxes reported here should not be compared with other reports
567 under different conditions.

568 **3.4 The back trajectory and PSCF analysis**

569 The discussion above suggested the regional transport from both Beijing and the
570 NCP have important influence on the air quality of the Yufa site. However, both the
571 bivariate polar plots and surface flux intensity calculation were based on the
572 observation data at a ground measurement site. Considering the limitation of
573 spatial representation of the Yufa site, the PSCF analysis based on the HYSPLIT-4
574 model was used to demonstrate the regional transport influence of the megacity
575 Beijing and the NCP on Yufa in this section.

Figure 9. here

Figure 10. here

PSCF analysis was used in this study by combining backward trajectories and the corresponding surface transport flux intensities of pollutants. PSCF results of SO_2, NO, NO_2, NO_x, CO, O_3 and O_x in 6-h time resolution are shown in Fig. 9 for positive influx intensities (i.e. from south to north) and Fig. 10 for negative outflux intensities (i.e. from north to south). It can be seen from Fig. 9, that the higher PSCF values for most pollutants are located at the area south-west to the Yufa site, which indicates the positive surface flux intensities of the Yufa site are consistent with the air masses moving from south to Yufa. Figure 10 shows the higher PSCF values for most pollutants are located at the area north to the Yufa site, which indicates the negative surface flux intensities of the Yufa site are consistent with the air masses moving from north to Yufa. The PSCF analysis results validate the calculated flux intensities based on observation data can be used to evaluate the regional transport influence of Beijing and the NCP on the Yufa site. However, it should be noticed that the PSCF results of NO, NO_2, and NO_x was inconsistent with the flux calculation results sometimes (Fig. 9 and 10), which may partially ascribe to the lifetime of these species is much shorter than 12 h. As a cross-boundary site between the megacity Beijing and the NCP, the surface flux intensities at the Yufa site may also indicate the transport between the megacity Beijing and the NCP.

3.5 Uncertainty and limitation

Uncertainty in calculation of the surface flux intensities in this study mainly comes from the measurement of the pollutants and the wind. Based on the instruments used, the uncertainty of the measurement of the concentrations of SO_2, NO_x, CO, and O_3 was within 10 %, 10 %, 1 %, and 5 %, respectively. The uncertainty of wind speed measurement was less than 5 % and the uncertainty of wind direction was about 1 %. Thus, the uncertainty of the overall surface flux intensity for SO_2, NO_x, CO, and O_3 was less than 12 %, 12 %, 6 %, and 8 %, respectively.

In this study, we did not intent to extrapolate from the Yufa site to the entire region. We focus on the method developing and evaluation of the regional transport influence of Beijing and the NCP on the cross-boundary site based on the ground-based observation data. Bivariate Polar plots analysis and surface flux intensity calculation were conducted, and we obtained clear evidences of surface pollutants transport from Beijing to the Yufa site and from the NCP to the Yufa site. Considering the variations of the vertical and horizontal distributions of the air pollutants and meteorological parameters, and the influence of the boundary layer on the regional transport, three dimensional observations with high precision and resolution are needed for further comprehensive discussion of the regional transport between Beijing and the NCP.

4. Conclusions

We used 2-year continuous observation data at a cross-boundary rural site between the megacity Beijing and the NCP to investigate regional transport influence on the Yufa site, as part of the “Campaign of Air Quality Research in Beijing and Surrounding Region 2006–2008” (CAREBeijing 2006–2008). The gaseous pollutants SO_2, NO, NO_2,

620 NO_x, CO, O_3, and O_x, together with meteorological data, were determined at Yufa
621 from August 2006 to October 2008. During the observation period, the average
622 concentrations of the pollutants at the Yufa site were relatively high, suggesting a
623 profound influence of the emissions from the megacity Beijing and regional transport
624 from the NCP.

625 Through bivariate polar plots, we found that the south wind, at relatively high
626 wind speed, was essential for the inflow of SO_2, CO, and O_3 from the NCP to Yufa. For
627 NO, NO_2, NO_x, and even CO, the emission from Beijing played a dominant role. The
628 seasonal variations of emission intensity, meteorological conditions, pollutant
629 lifetimes lead to the seasonal variations of the regional transport of pollutants, hence
630 the different bivariate polar plot patterns.

631 The the surface flux intensities showed strong net surface transport from the
632 NCP to Yufa in summer and net surface transport from Beijing to Yufa in winter,
633 mainly varied with the prevailing wind. The positive net influxes of SO_2, CO, and O_3
634 in this study indicate a northward regional transport of these species from the NCP.
635 Whereas the fluxes of NO_x indicate the influence of NO_x emission in Beijing city
636 could only influence downwind area adjacent to Beijing, due to the limited
637 transport distance of NO_x.

638 PSCF analysis demonstrated the regional transport from Beijing and the NCP to
639 Yufa can be evaluated by the surface flux intensity calculation based on the ground-
640 based measurement data. As a cross-boundary site between the megacity Beijing
641 and the NCP, the surface transport flux intensities at the Yufa site may also indicate
642 the transport between the megacity Beijing and the NCP.

643 Our results again suggested that Beijing and the NCP have tight interactions
644 through regional transport of air pollutants. Factors affecting the transport flux such
645 as meteorological parameters, especially wind speed and wind direction, emissions
646 inventory, and photochemical reactions are essential for the regional transport fluxes
647 and thus the air quality of the megacity Beijing and its surrounding areas. Therefore,
648 both local emissions reduction and regional cooperative control should be taken
649 considered in air quality management of Beijing.
650
651 **Author contribution**. T. Zhu designed the experiments and L. Zeng and the staff of
652 the Yufa site carried out the experiment. Y. Li conducted the data analysis with
653 contributions from all co-authors. J. Liu provided the emission maps. J. Wang
654 managed the observation data of the program. Y. Li prepared the manuscript with
655 the help of T. Zhu, C. Ye, J. Liu and Y. Zhu.
656 **Data availability.** The observation data of the Yufa site used in this paper is available
657 on requests.
658 **Acknowledgements.** The authors express their sincere thanks to the staff of the Yufa
659 site for carrying out the measurements. This work as part of CAREBeijing (Campaign
660 of Atmospheric Researches in Beijing and surrounding area) was supported by Beijing
661 Council of Science and Technology. This study was also supported by the National
662 Natural Science Foundation Committee of China (21190051, 41121004, 41421064),
663 the European 7th Framework Programme Project PURGE (265325), the Collaborative
664 Innovation Center for Regional Environmental Quality.

665 **References**

666 An, X., Zhu, T., Wang, Z., Li, C., and Wang, Y.: A modeling analysis of a heavy air
667 pollution episode occurred in Beijing, Atmos. Chem. Phys., 7, 3103-3114, doi:
668 10.5194/acp-7-3103-2007, 2007.

669 Ashbaugh, L. L., Malm, W. C., Sadeh, W. Z.: A residence time probability analysis of
670 sulfur concentrations at Grand Canyon National Park. Atmos. Environ., 19 (8),
671 1263–1270,1985.

672 Beirle, S., Boersma, K. F., Platt, U., Lawrence, M. G., and Wagner, T.: Megacity
673 emissions and lifetimes of nitrogen oxides probed from space, Science, 333,
674 1737-1739, doi:10.1126/science.1207824, 2011.

675 Beirle, S., Hörmann, C., Penning de Vries, M., Dörner, S., Kern, C., and Wagner, T.:
676 Estimating the volcanic emission rate and atmospheric lifetime of SO_2 from
677 space: a case study for Kīlauea volcano, Hawai`i, Atmos. Chem. Phys., 14, 8309-
678 8322, doi:10.5194/acp-14-8309-2014, 2014.

679 Carslaw, D. C., Beevers, S. D., Ropkins, K., and Bell, M. C.: Detecting and quantifying
680 aircraft and other on-airport contributions to ambient nitrogen oxides in the
681 vicinity of a large international airport, Atmos. Environ., 40, 5424-5434, 2006.

682 Chen, H. S., Li, J., Ge, B. Z., Yang, W. Y., Wang, Z. F., Huang, S., Wang, Y. L., Yan, P. Z.,
683 Li, J. J., Zhu, L. L., Modeling study of source contributions and emergency
684 control effects during a severe haze episode over the Beijing-Tianjin-Hebei area.
685 SCIENCE CHINA Chemistry, 58 (9): 1403-1415, 2015.

686 China Statistical Yearbook 2008 (Beijing: China Statistic Press) (in Chinese).

687 Gu, D., Wang, Y., Smeltzer, C., and Liu, Z.: Reduction in NO_x Emission Trends over
688 China: Regional and Seasonal Variations, Environ. Sci. Technol., 47, 12912-
689 12919, doi:10.1021/es401727e, 2013.

690 Guo, S., Hu, M., Wang, Z. B., Slanina, J., and Zhao, Y. L.: Size-resolved aerosol water-
691 soluble ionic compositions in the summer of Beijing: implication of regional

692 secondary formation, Atmos. Chem. Phys., 10, 947-959, doi:10.5194/acp-10-
693 947-2010, 2010.

694 He, H., Li, C., Loughner, C. P., Li, Z., Krotkov, N. A., Yang, K., Wang, L., Zheng, Y., Bao,
695 X., Zhao, G., and Dickerson, R. R.: SO_2 over central China: Measurements,
696 numerical simulations and the tropospheric sulfur budget, J. Geophys. Res.-
697 Atmos., 117, D00K37, doi:10.1029/2011JD016473, 2012.

698 Henry, R. C., Chang, Y. -S., and Spiegelman, C. H.: Locating nearby sources of air
699 pollution by nonparametric regression of atmospheric concentrations on wind
700 direction, Atmos. Environ., 36, 2237-2244, 2002.

701 Jayamurugan, R., Kumaravel, B., Palanivelraja, S., and Chockalingam, M. P.: Influence
702 of Temperature, Relative Humidity and Seasonal Variability on Ambient Air
703 Quality in a Coastal Urban Area, International Journal of Atmospheric Sciences,
704 2013, 1-7, doi:10.1155/2013/264046, 2013.

705 Lee, C., Martin, R. V., van Donkelaar, A., Lee, H., Dickerson, R. R., Hains, J. C., Krotkov,
706 N., Richter, A., Vinnikov, K., and Schwab, J. J.: SO_2 emissions and lifetimes:
707 Estimates from inverse modeling using in situ and global, space-based
708 (SCIAMACHY and OMI) observations, J. Geophys. Res., 116, D06304,
709 doi:10.1029/2010jd014758, 2011.

710 Lin, W., Xu, X., Zhang, X., and Tang, J.: Contributions of pollutants from North China
711 Plain to surface ozone at the Shangdianzi GAW Station, Atmos. Chem. Phys., 8,
712 5889-5898, doi:10.5194/acp-8-5889-2008, 2008.

713 Lin, W., Xu, X., Ge, B., and Zhang, X.: Characteristics of gaseous pollutants at
714 Gucheng, a rural site southwest of Beijing, J. Geophys. Res., 114, D00G14,
715 doi:10. 1029/2008JD010339, 2009.

716 Lin, W., Xu, X., Ge, B., and Liu, X.: Gaseous pollutants in Beijing urban area during the
717 heating period 2007–2008: variability, sources, meteorological, and chemical
718 impacts, Atmos. Chem. Phys., 11, 8157-8170, doi:10.5194/acp-11-8157-2011,
719 2011.

720 Liu, J., Mauzerall, D. L., Chen, Q., Zhang, Q., Song, Y., Peng, W., Klimont, Z., Qiu, X.,
721 Zhang, S., Hu, M., Lin, W., Smith, K. R., and Zhu, T.: Air pollutant emissions from
722 Chinese households: A major and underappreciated ambient pollution source,
723 Proc. Natl. Acad. Sci., 113, 7756-7761, 10.1073/pnas.1604537113, 2016.

724 Matsui, H., Koike, M., Kondo, Y., Takegawa, N., Kita, K., Miyazaki, Y., Hu, M., Chang, S.
725 Y., Blake, D. R., Fast, J. D., Zaveri, R. A., Streets, D. G., Zhang, Q., and Zhu, T.:
726 Spatial and temporal variations of aerosols around Beijing in summer 2006:
727 Model evaluation and source apportionment, J. Geophys. Res.-Atmos., 114,
728 D00G13, doi:10.1029/2008JD010906, 2009.

729 Parrish, D. D., and Zhu, T.: Clean Air for Megacities, Science, 326, 674-675,
730 doi:10.1126/science.1176064, 2009.

731 Qin, M., Xie, P. H., Wu, D. X., Xu, J., Si, F. Q., Wang, M. H., Dou, K., Zhang, Y., Xiao, X.,
732 Liu, W. S., Liu, S. S., Wang, F. P., Fang, W., Liu, J. G., and Liu, W. Q.: Investigation
733 of variation characteristics and levels of SO_2-NO_2-O_3 and PM_{10} in Beijing during
734 2008 Olympic Games, J. Atmos. Environ. Opt., 4, 329-340, 2009.

735 Shao, M., Tang, X., Zhang, Y., and Li, W.: City Clusters in China: Air and Surface Water
736 Pollution, Front. Ecol. Environ., 4, 353-361, 2006.

737 Sander, S. P., J. Abbatt, J. R. Barker, J. B. Burkholder, R. R. Friedl, D. M. Golden, R. E.
738 Huie, C. E. Kolb, M. J. Kurylo, G. K. Moortgat, V. L. Orkin and P. H. Wine
739 "Chemical Kinetics and Photochemical Data for Use in Atmospheric Studies,
740 Evaluation No. 17," JPL Publication 10-6, Jet Propulsion Laboratory, Pasadena,
741 http://jpldataeval.jpl.nasa.gov, 2011.

742 Streets, D. G., Fu, J. S., Jang, C. J., Hao, J., He, K., Tang, X., Zhang, Y., Wang, Z., Li, Z.,
743 Zhang, Q., Wang, L., Wang, B., and Yu, C.: Air quality during the 2008 Beijing
744 Olympic Games, Atmos. Environ., 41, 480-492,2007.

745 Takegawa, N., Miyakawa, T., Kuwata, M., Kondo, Y., Zhao, Y., Han, S., Kita, K., Miyazaki,
746 Y., Deng, Z., Xiao, R., Hu, M., van Pinxteren, D., Herrmann, H., Hofzumahaus, A.,
747 Holland, F., Wahner, A., Blake, D. R., Sugimoto, N., and Zhu, T.: Variability of

748 submicron aerosol observed at a rural site in Beijing in the summer of 2006, J.
749 Geophys. Res., 114, D00G05, doi:10.1029/2008jd010857, 2009.

750 Tang, X. Y.: The characteristics of urban air pollution in China, in Urbanization, Energy,
751 and Air Pollution in China, pp. 47-54, Natl. Acad. Press, Washington, D. C.,2004.

752 Wang, M., Zhu, T., Zheng, J., Zhang, R. Y., Zhang, S. Q., Xie, X. X., Han, Y. Q., and Li, Y.:
753 Use of a mobile laboratory to evaluate changes in on-road air pollutants during
754 the Beijing 2008 Summer Olympics, Atmos. Chem. Phys., 9, 8247-8263,
755 doi:10.5194/acp-9-8247-2009, 2009.

756 Wang, M., Zhu, T., Zhang, J. P., Zhang, Q. H., Lin, W. W., Li, Y., and Wang, Z. F.: Using a
757 mobile laboratory to characterize the distribution and transport of sulfur dioxide
758 in and around Beijing, Atmos. Chem. Phys., 11, 11631-11645, doi:10.5194/acp-
759 11-11631-2011, 2011.

760 Wang, S., Li, G. G., Gong, Z. Y., Du, L., Zhou, Q. T., Meng, X. Y., Xie, S. Y., Zhou. L.,
761 Spatial distribution, seasonal variation and regionalization of $PM_{2.5}$
762 concentrations in China. SCIENCE CHINA Chemistry, 58 (9): 1435-1443, 2015.

763 Wang, T., Ding, A., Gao, J., and Wu, W. S.: Strong ozone production in urban plumes
764 from Beijing, China, Geophys. Res. Lett., 33, L21806, doi:10.1029/2006GL02
765 7689, 2006.

766 Wang, T., Nie, W., Gao, J., Xue, L. K., Gao, X. M., Wang, X. F., Qiu, J., Poon, C. N.,
767 Meinardi, S., Blake, D., Wang, S. L., Ding, A. J., Chai, F. H., Zhang, Q. Z., and
768 Wang, W. X.: Air quality during the 2008 Beijing Olympics: secondary pollutants
769 and regional impact, Atmos. Chem. Phys., 10, 7603–7615, doi:10.5194/acp-10-
770 7603-2010, 2010.

771 Wang, Y. Q., Zhang, X. Y., and Draxler, R. R.: TrajStat: GIS-based software that uses
772 various trajectory statistical analysis methods to identify potential sources from
773 long-term air pollution measurement data, Environmental Modelling &
774 Software, 24, 938-939, doi:10.1016/j.envsoft.2009.01.004, 2009.

775 Wehner, B., Birmili, W., Ditas, F., Wu, Z., Hu, M., Liu, X., Mao, J., Sugimoto, N., and
776 Wiedensohler, A.: Relationships between submicrometer particulate air
777 pollution and air mass history in Beijing, China, 2004–2006, Atmos. Chem. Phys.,
778 8, 6155-6168, doi:10.5194/acp-8-6155-2008, 2008.

779 Westmoreland, E. J., Carslaw, N., Carslaw, D. C., Gillah, A., and Bates, E.: Analysis of
780 air quality within a street canyon using statistical and dispersion modelling
781 techniques, Atmos. Environ., 41, 9195-9205, 2007.

782 White, W. H., Anderson, J. A., Blumenthal, D. L., Husar, R. B., Gillani, N. V., Husar, J. D.,
783 and Wilson, W. E.: Formation and transport of secondary air pollutants: ozone
784 and aerosols in the St. Louis urban plume, Science, 194, 187–189, 1976.

785 Wu, Q. Z., Wang, Z. F., Gbaguidi, A., Gao, C., Li, L. N., and Wang, W.: A numerical
786 study of contributions to air pollution in Beijing during CAREBeijing-2006,
787 Atmos. Chem. Phys., 11, 5997-6011, doi:10.5194/acp-11-5997-2011, 2011.

788 Xu, J., Ma, J. Z., Zhang, X. L., Xu, X. B., Xu, X. F., Lin, W. L., Wang, Y., Meng, W., and Ma,
789 Z. Q.: Measurements of ozone and its precursors in Beijing during summertime:
790 impact of urban plumes on ozone pollution in downwind rural areas, Atmos.
791 Chem. Phys., 11, 12241-12252, doi:10.5194/acp-11-12241-2011, 2011.

792 Xu, X., Zhou, L., Zhou, X., Yan, P., Weng, Y., Tao, S., Mao, J., Ding, G., Bian, L., and Jhon,
793 C.: Influencing domain of peripheral sources in the urban heavy pollution
794 process of Beijing, Science in China, 48, 565-575, 2005.

795 Yuan, Z., Lau, A. K. H., Shao, M., Louie, P. K. K., Liu, S. C., and Zhu, T.: Source analysis
796 of volatile organic compounds by positive matrix factorization in urban and rural
797 environments in Beijing, J. Geophys. Res., 114, D00G15, doi:10.1029/2008
798 jd011190, 2009.

799 Zhang, J. P., Zhu, T., Zhang, Q. H., Li, C. C., Shu, H. L., Ying, Y., Dai, Z. P., Wang, X., Liu,
800 X. Y., Liang, A. M., Shen, H. X., and Yi, B. Q.: The impact of circulation patterns on
801 regional transport pathways and air quality over Beijing and its surroundings,
802 Atmos. Chem. Phys., 12, 5031-5053, doi:10.5194/acp-12-5031-2012, 2012.

Zhang, Q., Yuan, B., Shao, M., Wang, X., Lu, S., Lu, K., Wang, M., Chen, L., Chang, C. C., and Liu, S. C.: Variations of ground-level O_3 and its precursors in Beijing in summertime between 2005 and 2011, Atmos. Chem. Phys., 14, 6089-6101, doi:10.5194/acp-14-6089-2014, 2014.

Zhang, R., Jing, J., Tao, J., Hsu, S. C., Wang, G., Cao, J., Lee, C. S. L., Zhu, L., Chen, Z., Zhao, Y., and Shen, Z.: Chemical characterization and source apportionment of $PM_{2.5}$ in Beijing: seasonal perspective, Atmos. Chem. Phys., 13, 7053-7074, doi: 10.5194/acp-13-7053-2013, 2013.

Zhou, Y., Wu, Y., Yang, L., Fu, L., He, K., Wang, S., Hao, J., Chen,J., and Li, C.: The impact of transportation control measures on emission reductions during the 2008 Olympic Games in Beijing, China, Atmos. Environ., 44, 285–293, 2010.

Zhu, L., Huang, X., Shi, H., Cai, X., and Song, Y.: Transport pathways and potential sources of PM_{10} in Beijing, Atmos. Environ., 45, 594-604, 2011.

Zhu, Y., Zhang, J., Wang, J., Chen, W., Han, Y., Ye, C., Li, Y., Liu, J., Zeng, L., Wu, Y., Wang, X., Wang, W., Chen, J., and Zhu, T.: Distribution and sources of air pollutants in the North China Plain based on on-road mobile measurements, Atmos. Chem. Phys., 16, 12551-12565, doi:10.5194/acp-16-12551-2016, 2016.

828 **Table 1.** The overview of measurement instruments.

Species/ Parameter	Instrument	Detection limit	Time resolution	Precision	Uncertainty
SO_2	Ecotech 9850B	0.5 ppb	1 min	0.5% (0.5 ppb)	10%
NO-NO_x	Ecotech 9841B	0.5 ppb	1 min	1% (0.5 ppb)	10%
CO	Ecotech 9830	50 ppb	1 min	1% (0.1 ppm)	1%
O_3	Ecotech 9810B	0.4 ppb	1 min	0.5% (1 ppb)	5%
WS	LASTEM	-	10 min	0,1 m s^{-1}	5%
WD	LASTEM	-	10 min	0,1 º	1%
BP	LASTEM	-	10 min	0,1 hPa	±0.35 hPa
T	LASTEM	-	10 min	0,1 °C	±0.2°C
RH	LASTEM	-	10 min	1%	±3%

829

830 **Table 2.** The total and seasonal net surface flux intensities (mean ± SD) (μg s^{-1} m^{-2}) of

831 gaseous pollutants at the Yufa site from 1 September 2006 to 31 August 2008.

Flux (μg s^{-1} m^{-2})	SO_2	NO	NO_2	NO_x	CO	O_3	O_x
Autumn_06	5.3±79.6	-6.3±27.5	-3±60.2	-9.4±78.9	-30±2730	19.4±128.8	25.9±177.6
Autumn_07	6.3±78.8	-6.6±33.6	-3.5±74.3	-10.1±98.6	-60±2570	10±120	6.6±170.3
Winter_06/07	11.8±139.1	-6.9±47.7	3.6±105.6	-3.3±142.9	350±4150	-11.9±127.5	-8.3±188
winter_07/08	-13.1±113.3	-11.5±46.5	-11±82.3	-22.6±117.6	-550±3380	-29.6±143.1	-40.7±191.2
Spring_07	11.3±90.5	-1.9±12.1	0.1±71.1	-1.9±78.8	50±2720	3.4±261.8	3.5±315.5
Spring_08	13.5±92	-1.8±15.2	0.2±76.4	-1.5±87	160±2630	10.7±266.4	10.9±321.2
Summer_07	11±35.3	0.4±6.7	8.4±46.9	8.7±51.5	600±1960	71.3±175.7	79.7±211.4
Summer_08	5.7±26.1	0.1±4.9	1±32.7	1.1±36.6	120±1540	48.1±183.3	49.1±207.8
Total	6.2±89.5	-4.3±29.5	-0.6±72.3	-4.9±93	70±2830	14.7±187.8	14.8±234.9

832

833 **Table 3a.** The total and seasonal surface influx intensities (mean±SD) (positive; from

834 the NCP to Yufa, μg s^{-1} m^{-2}) of gaseous pollutants at the Yufa site from 1 September

835 2006 to 31 August 2008.

Influx (μg s^{-1} m^{-2})	SO_2	NO	NO_2	NO_x	CO	O_3	O_x
Autumn_06	53.3±62.7	5.1±7.9	42.5±34.3	47.6±37.9	1770±1740	85±131.6	143.1±158.3
Autumn_07	43.9±80.8	8.5±14.5	48.7±51.8	57.2±60.7	1720±1820	65.1±116.8	117.3±140.2
Winter_06/07	106.3±126.1	19.8±30	82.3±83	102±101.5	3360±3620	40.1±74.1	122.4±112.8
winter_07/08	72.3±95.1	13.6±20.9	60.4±60.2	74±72.6	2170±2130	41.7±70.2	102.1±98.3
Spring_07	62.9±88.3	3.8±7.2	53.6±46.6	57.5±49.7	1970±2050	158.8±193.2	212.5±223.1
Spring_08	64.7±97.5	6±9	56.8±44.6	62.7±49.1	2090±1850	162.5±194.4	222.9±217.9
Summer_07	22.3±38.7	2.9±5.4	32.4±30.1	35.3±32.4	1560±1630	140.7±177.9	173.1±199.7
Summer_08	18.9±24.3	2.8±2.6	20.8±16.3	23.6±18.2	1060±880	138.2±168.9	160.1±180.2
Total	53.2±84.8	7.4±15.4	48.3±51.5	55.8±60.7	1920±2130	108.2±159.2	159.7±180

836 **Table 3b.** The total and seasonal outflux intensities (mean ± SD) (negative; from

837 Beijing to Yufa, μg s^{-1} m^{-2}) of gaseous pollutants at the Yufa site from 1 September

838 2006 to 31 August 2008.

Outflux ($\mu g\ s^{-1}\ m^{-2}$)	SO_2	NO	NO_2	NO_x	CO	O_3	O_x
Autumn_06	-40.4±66	-17.8±34.4	-48.6±43.9	-66.4±67.3	-1830±2360	-44.7±87.5	-91.2±103.4
Autumn_07	-30.2±56.5	-21.4±39.9	-54.5±54.9	-75.9±82.9	-1800±1910	-48.9±92.3	-101.5±120.4
Winter_06/07	-72.8±86	-30.7±48.1	-66.8±67.6	-97.6±103.8	-2350±2380	-58.4±146.3	-125.2±163.9
winter_07/08	-73.9±81.6	-29.5±51.2	-61.9±52.9	-91.3±92.4	-2490±2690	-80.4±159.2	-142.3±175.7
Spring_07	-41.3±55.8	-7.8±13.2	-54.6±45.6	-62.4±52.6	-1920±1720	-155.2±225	-209.8±245.6
Spring_08	-38.8±44.4	-9.7±16.2	-57.4±56.4	-67.1±65.8	-1820±1660	-151.3±235.8	-205.2±259.7
Summer_07	-9±13.3	-4.2±6.5	-34.2±40.8	-38.4±44.9	-1110±1210	-51.6±76.6	-85.8±102.2
Summer_08	-12.1±15.8	-3.5±5	-25.6±30.1	-29.1±33.3	-1150±1320	-75.2±119.5	-100.1±137.1
Total	-42.8±64.6	-16.7±35.2	-52±52.8	-68.7±77.1	-1870±2080	-85±163.2	-137.3±184.5

Table 4. The mean net surface flux intensities (i.e. Flux_2007 and Flux_2008), the influx intensities (positive; from the NCP to Yufa; In_2007 and In_2008), the outflux intensities (negative; from Beijing to Yufa; Out_2007 and Out_2008), and the mean concentrations (i.e. Cont._2007 and Cont._2008) during the 2008 Beijing Olympic period (from 8 August 2008 to 20 September 2008) and the same corresponding period of 2007 (from 8 August 2007 to 20 September 2007).

Flux ($\mu g\ s^{-1}\ m^{-2}$)	Flux_2007	In_2007	Out_2007	Flux_2008	In_2008	Out_2008	Cont._2007 (ppb)	Cont._2008 (ppb)
SO_2	7.9±19.3	14.9±20.8	-4.5±4.6	1.4±15.5	11.9±13.6	-9±8.8	3.6±3.4	3.9±2.2
NO	0.3±8.6	3.8±5	-5.9±9.9	-0.1±3.2	2.4±1.8	-2.5±2.3	4.3±5.5	1.9±0.6
NO_2	4.1±37.9	24.1±18.6	-31.3±37.9	-1.3±21.9	15.2±11.6	-17.5±17.1	16.1±10.2	8.5±3.6
NO_x	4.4±44.5	27.8±20.7	-37.2±45.3	-1.4±25	17.5±13.2	-20±19.2	20.5±13.3	10.4±4
CO	540±158	1390±1160	-980±980	10±1110	870±670	-850±740	1190±490	750±260
O_3	60±130	117.9±122.6	-42.6±61.1	24.9±124.6	110.9±111	-60.6±63.7	41.1±30.5	38.9±25.8
O_x	64.1±154.4	141.9±129.1	-73.9±82.4	23.7±142.1	126.7±118.4	-77.7±74.6	57.2±27.3	47.4±24.1

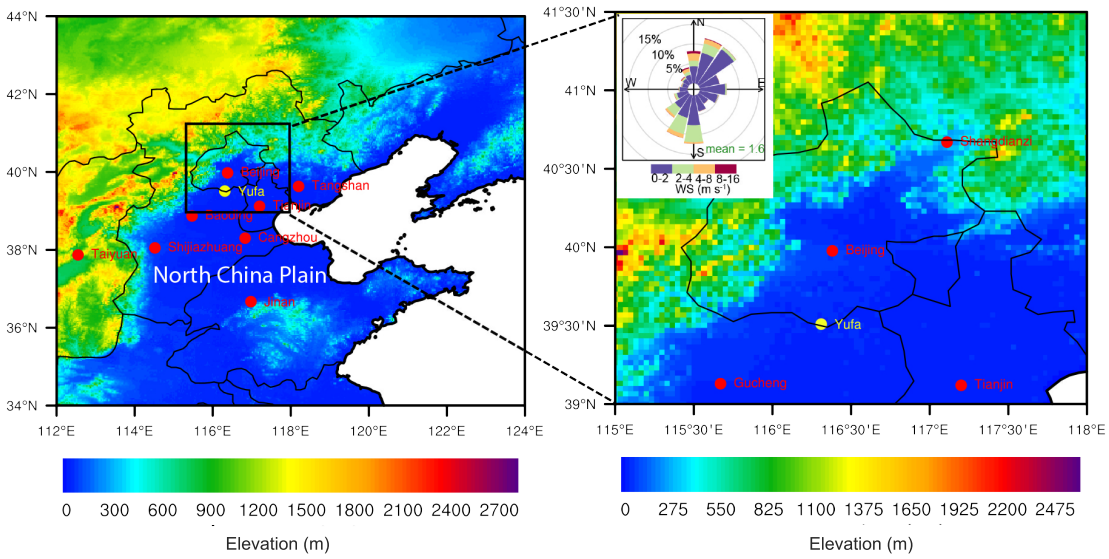

846

847 **Figure 1.** The location information of the Yufa site.

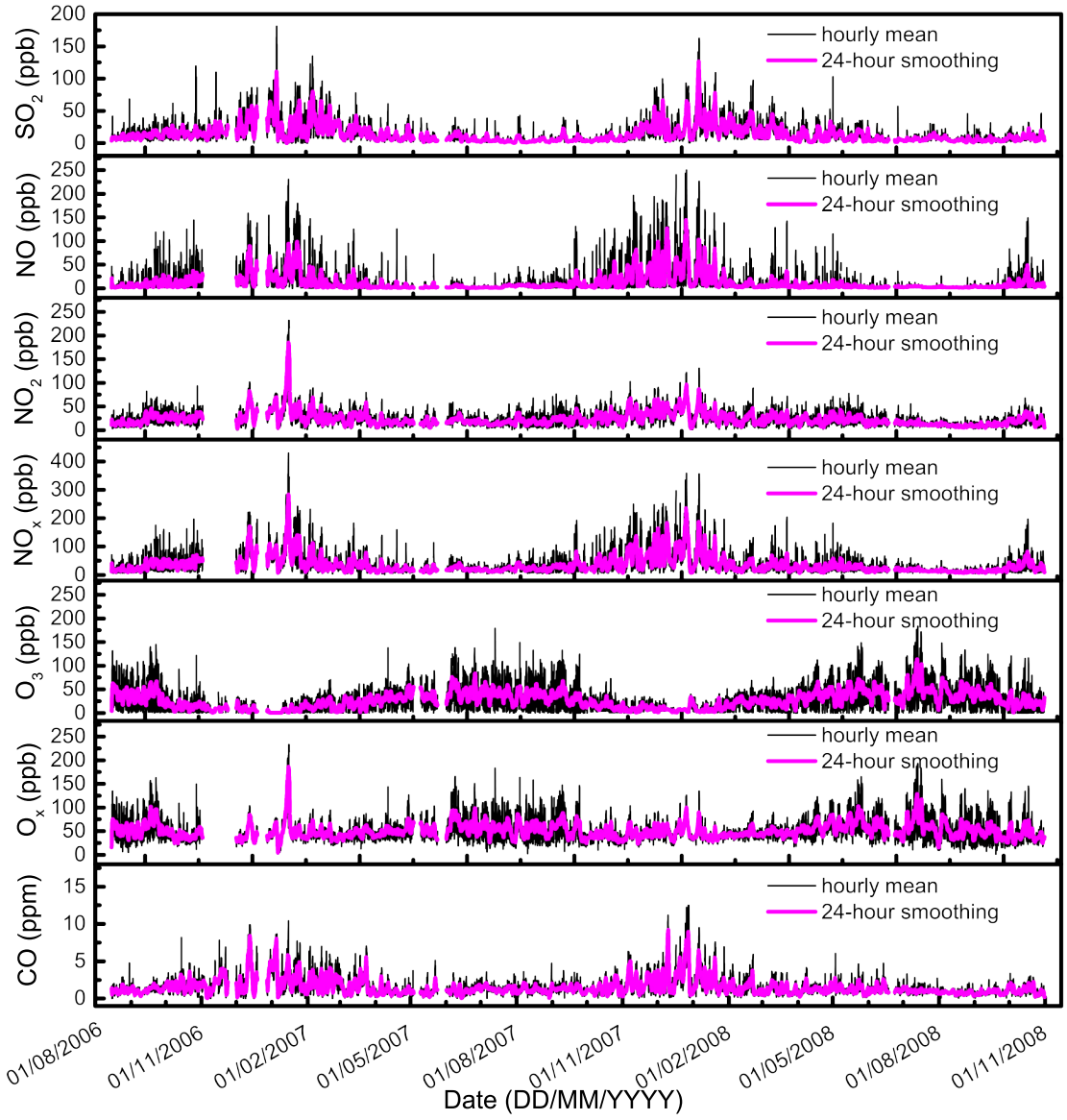

848

849 **Figure 2.** Time series of hourly mean (black line) and 24-hour smoothing

850 concentrations (red line) of SO_2, NO, NO_2, NO_x, O_3, O_x, and CO at the Yufa site from 15

851 August 2006 to 31 October 2008.

852

853

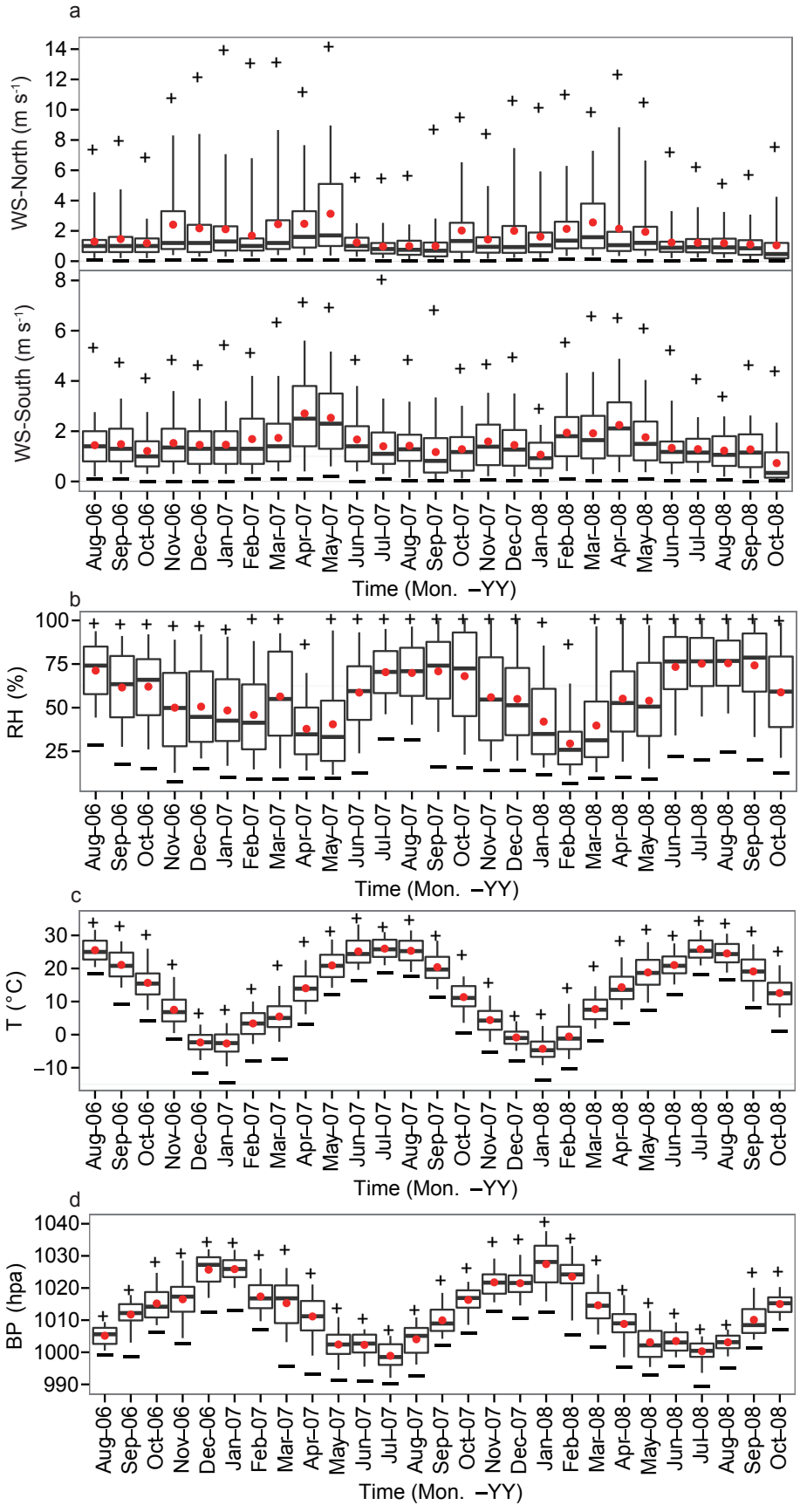
a
WS-North (m s-1)
WS-South (m s-1)
Time (Mon. –YY)
b
RH (%)
Time (Mon. –YY)
c
T (°C)
Time (Mon. –YY)
d
BP (hpa)
Time (Mon. –YY)
Aug–06
Sep–06
Oct–06
Nov–06
Dec–06
Jan–07
Feb–07
Mar–07
Apr–07
May–07
Jun–07
Jul–07
Aug–07
Sep–07
Oct–07
Nov–07
Dec–07
Jan–08
Feb–08
Mar–08
Apr–08
May–08
Jun–08
Jul–08
Aug–08
Sep–08
Oct–08

854

Figure 3. Monthly statistics of wind speed (WS) for north wind (a) top and south wind (a) bottom, relative Humidity (RH) (b), temperature (T) (c) and barometric pressure (BP) (d) at the Yufa site. The red point represents the mean value. The black cross bar stands for the median value. The black box and whisker denote the 5th, 25th, 75th and 95th percentiles, respectively. The plus and minus symbols represent the maximum and minimum, respectively. It should be clarified that the North and South wind here is different from the wind direction definition in meteorology. The South wind here is the wind with direction from 90° to 270°, while the North wind is from 0° to 90° and from 270° to 360°.

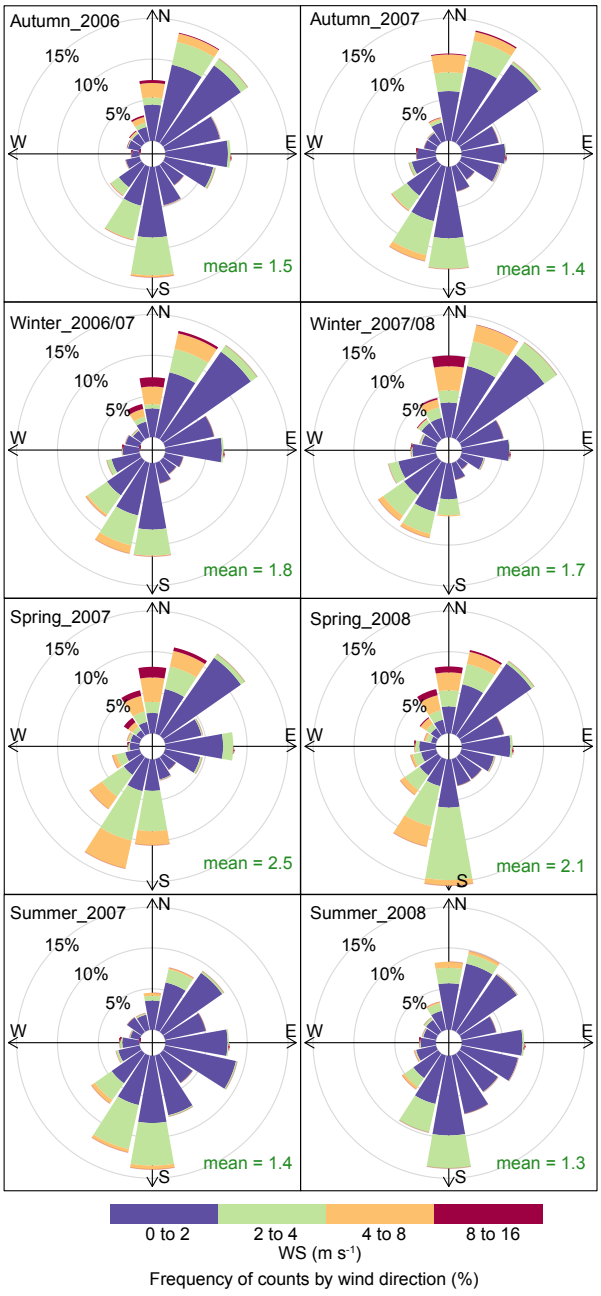

865

866 **Figure 4.** Wind rose plots based on frequencies of hourly data in Autmun_2006,
867 Autumn_2007, Winter_2006/07, Winter_2007/08, Spring_2007, Spring_2008,
868 Summer_2007, Summer_2008. Spring (MAM): March, April, and May; Summer (JJA):
869 June, July, and August; Autumn (SON): September, October, and November; Winter
870 (DJF): December, January, and February.

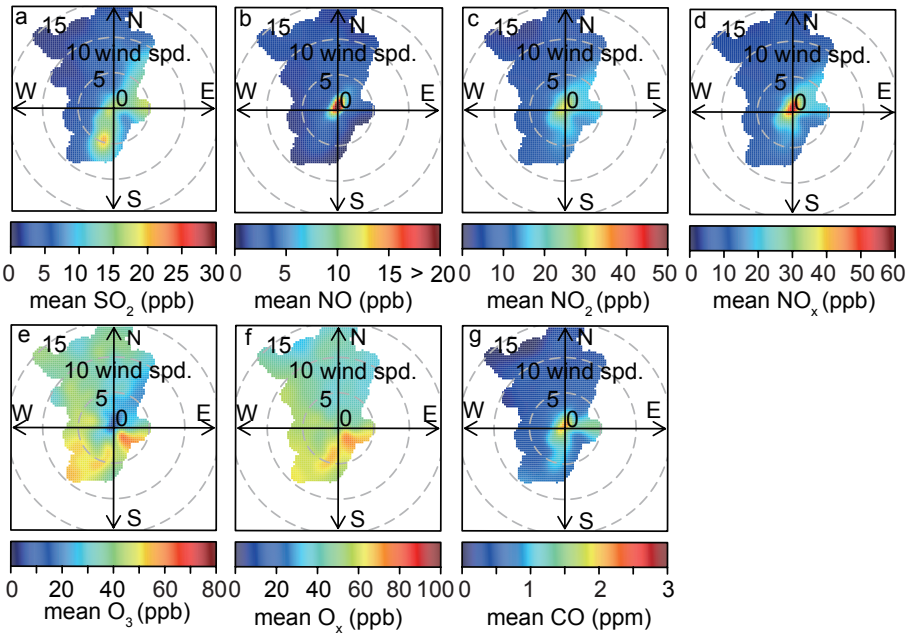

871

872 **Figure 5.** Bivariate polar plots for SO_2 (a), NO (b), NO_2 (c), NO_x (d), O_3 (e), O_x (f) and CO

873 (g) concentrations based on hourly average data at the Yufa site from 1 September

874 2006 to 31 August 2008. The colour scale shows the concentrations of pollutants in

875 ppb (or ppm specially for CO) and the radial scale shows the wind speed (m s^{-1}),

876 which increases from the centre of the plot radially outwards.

877

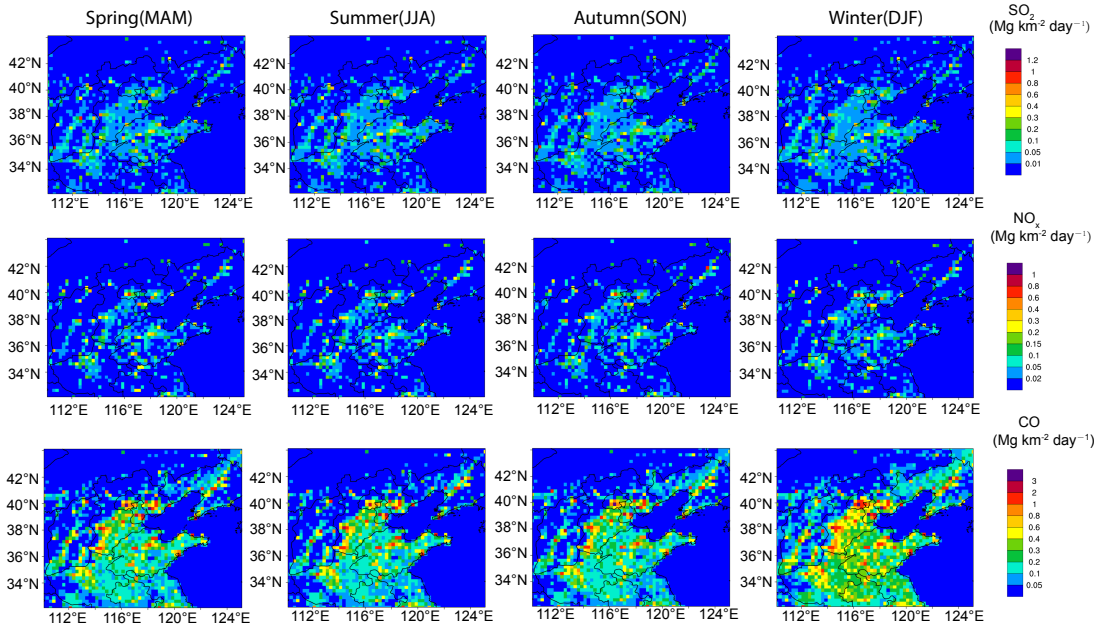

878

879 **Figure 6.** Spatial distribution of seasonal NO_x, CO, and SO_2 emissions in 2008 based

880 on the Multi-resolution Emission Inventory of China (MEIC; www.meicmodel.org)

881 (unit: Mg km^{-2} day^{-1}, horizontal resolution: 25 km×25 km).

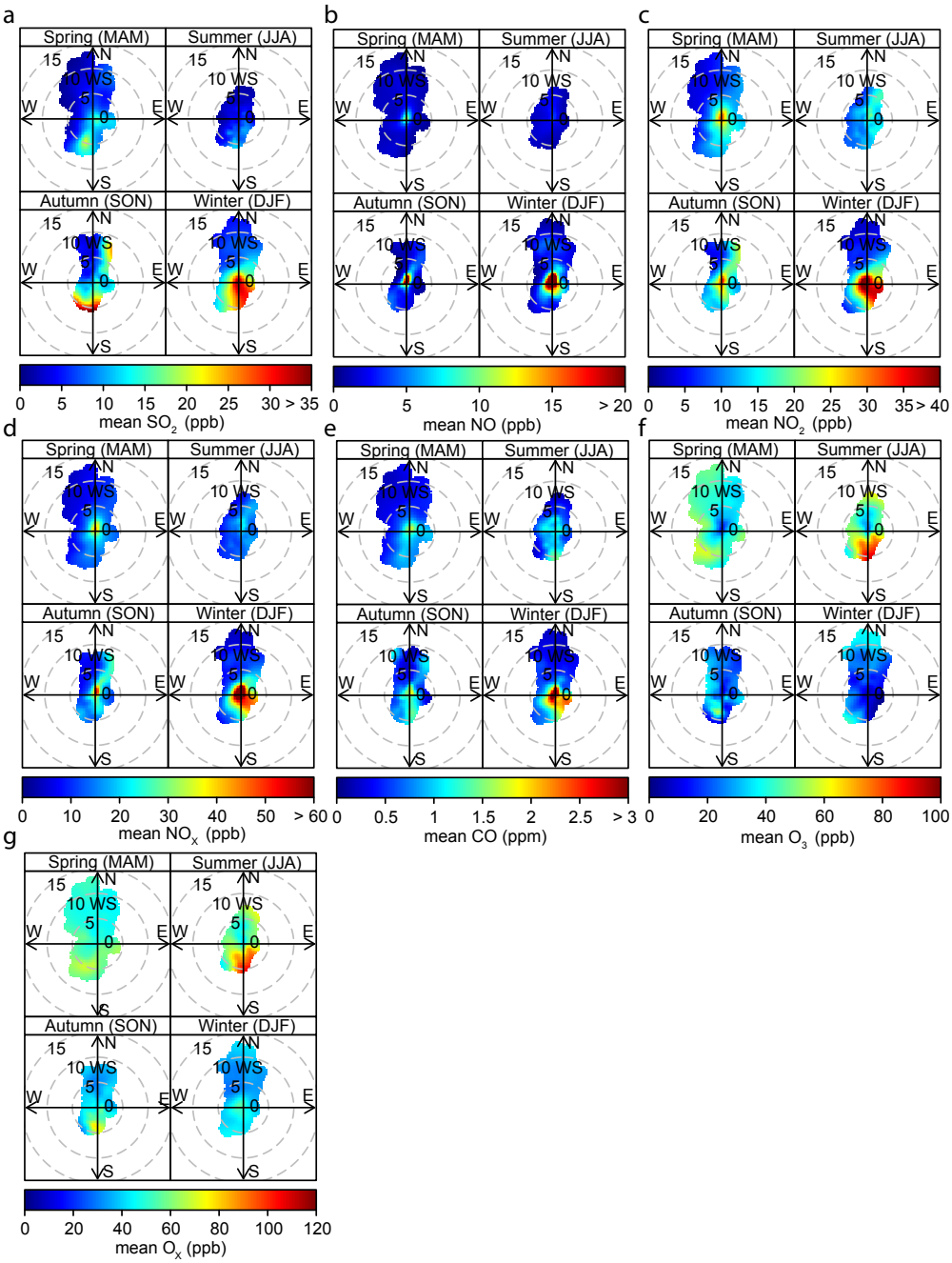

882

883 **Figure 7.** Seasonal bivariate polar plots for SO_2 (a), NO (b), NO_2 (c), NO_x (d), CO (e), O_3

884 (f), O_x (g) and concentrations based on hourly mean data at the Yufa site from 1

885 September 2006 to 31 August 2008. The colour scale shows the concentrations of

886 pollutants in ppb (or ppm specially for CO) and the radial scale shows the wind speed

887 (m s^{-1}), which increases from the centre of the plot radially outwards.

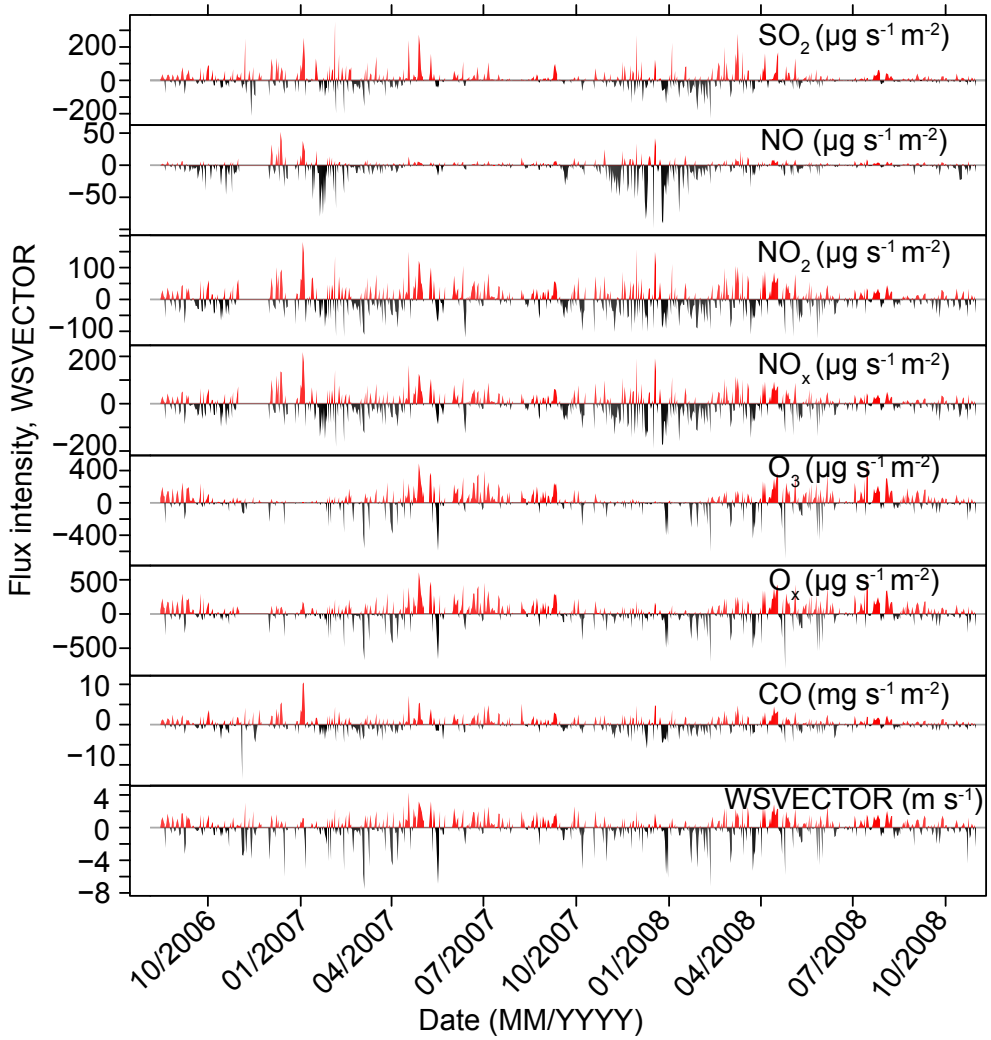

888

889 **Figure 8.** Time series of surface flux intensity (i.e. flux per unit cell, μg s^{-1} m^{-2} or mg
890 s^{-1} m^{-2}) for SO_2, NO, NO_2, NO_x, O_3, O_x, CO and wind vector (i.e. WSVECTOR=
891 $-\frac{1}{n}\sum_{j=1}^{n} WS_j \cdot cos\theta_j$, m s^{-1}) based on daily average data at the Yufa site from 15
892 August 2006 to 31 October 2008. The red shaded line indicates the positive transport
893 direction of gaseous pollutants from south to north (i.e. from the NCP to Yufa) and
894 the black shaded line represents the negative transport direction of gaseous
895 pollutants from north to south (i.e. from Beijing to Yufa).

896

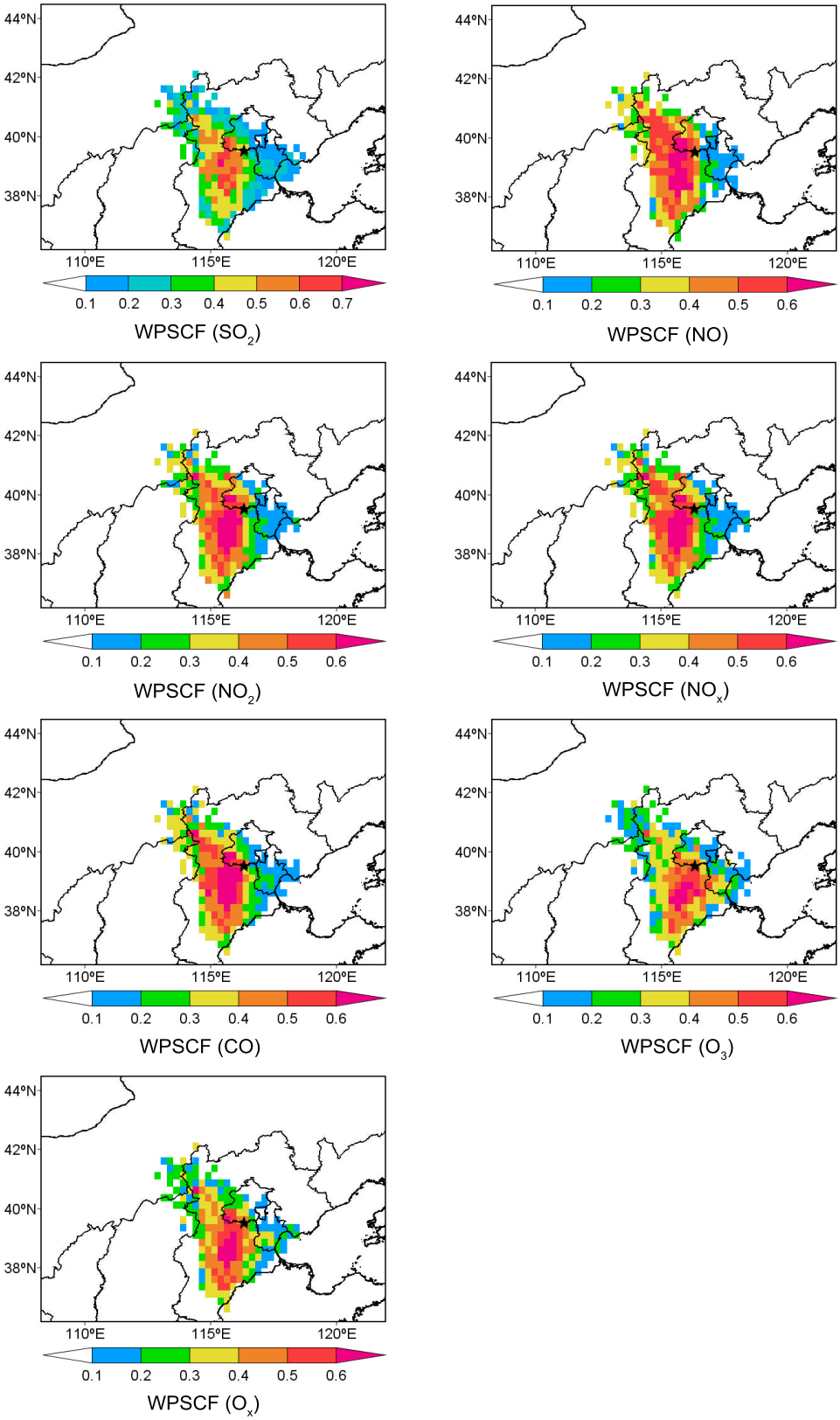
44°N
42°N
40°N
38°N
110°E
115°E
120°E
0.1 0.2 0.3 0.4 0.5 0.6 0.7
WPSCF (SO2)
0.1 0.2 0.3 0.4 0.5 0.6
WPSCF (NO)
0.1 0.2 0.3 0.4 0.5 0.6
WPSCF (NO2)
0.1 0.2 0.3 0.4 0.5 0.6
WPSCF (NOx)
0.1 0.2 0.3 0.4 0.5 0.6
WPSCF (CO)
0.1 0.2 0.3 0.4 0.5 0.6
WPSCF (O3)
0.1 0.2 0.3 0.4 0.5 0.6
WPSCF (Ox)

897

898 **Figure 9.** The PSCF maps for the SO_2 (a), NO (b), NO_2 (c), NO_x (d), O_3 (e), O_x (f) and CO
899 (g) surface influx intensity (positive; from the NCP to Yufa). The criterion value of the
900 surface flux intensity is set to greater than the median values, i.e. 20, 3, 30, 34, 40, 94,
901 and 1200 μg s^{-1} m^{-2} for SO_2, NO, NO_2, NO_x, O_3, O_x, and CO, respectively.

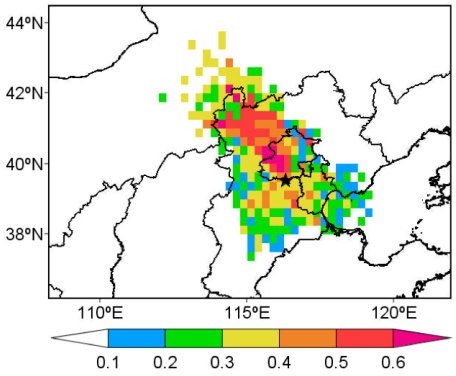

WPSCF (SO_2)

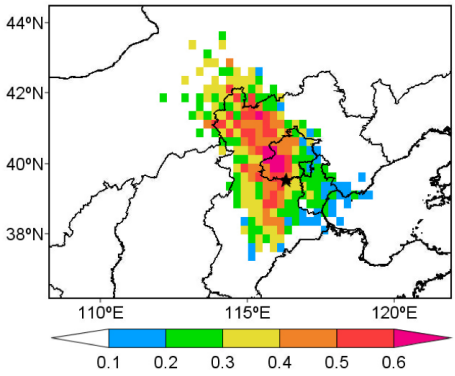

WPSCF (NO)

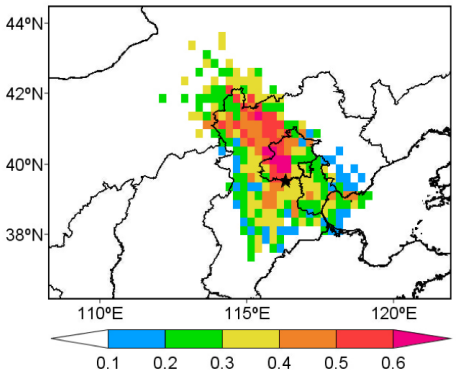

WPSCF (NO_2)

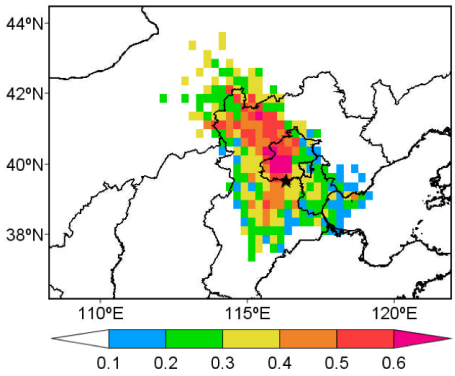

WPSCF (NO_x)

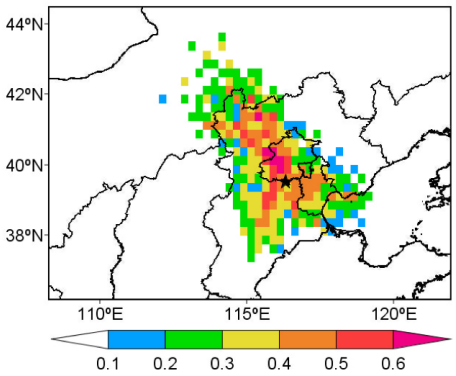

WPSCF (CO)

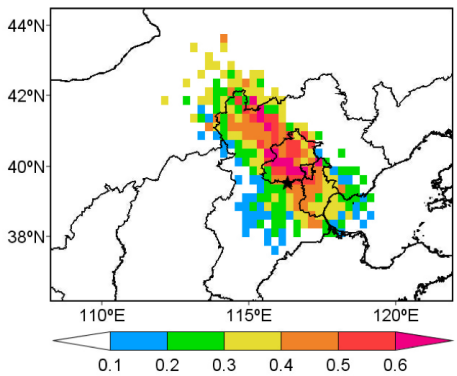

WPSCF (O_3)

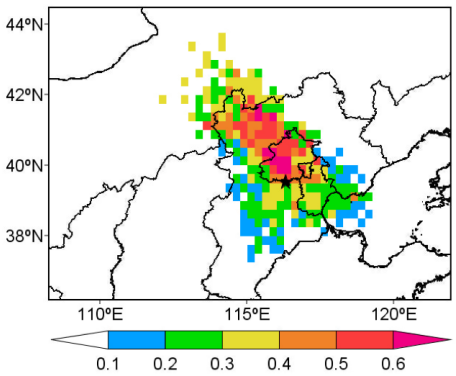

WPSCF (O_x)

902

Figure 10. The PSCF maps for the SO_2 (a), NO (b), NO_2 (c), NO_x (d), O_3 (e), O_x (f) and CO (g) surface outflux intensity (negative; from Beijing to Yufa). The criterion value of the surface flux intensity is set to lower than the median values, i.e. -18, -5, -35, -43, -16, -67, and -1200 μg s^{-1} m^{-2} for SO_2, NO, NO_2, NO_x, O_3, O_x, and CO, respectively.